



# CHORUS

This is the accepted manuscript made available via CHORUS. The article has been published as:

## Effects of optical polarization on hybridization of radiative and evanescent field modes

Andrii Iurov, Danhong Huang, Godfrey Gumbs, Wei Pan, and A. A. Maradudin

Phys. Rev. B **96**, 081408 — Published 23 August 2017

DOI: [10.1103/PhysRevB.96.081408](https://doi.org/10.1103/PhysRevB.96.081408)

# Effects of Optical Polarization on Hybridization of Radiative and Evanescent Field Modes

Andrii Iurov<sup>1</sup>, Danhong Huang<sup>2</sup>, Godfrey Gumbs<sup>3</sup>, Wei Pan<sup>4</sup> and A. A. Maradudin<sup>5</sup>

<sup>1</sup>*Center for High Technology Materials, University of New Mexico,  
1313 Goddard SE, Albuquerque, New Mexico, 87106, USA*

<sup>2</sup>*Air Force Research Laboratory, Space Vehicles Directorate,  
Kirtland Air Force Base, New Mexico 87117, USA*

<sup>3</sup>*Department of Physics and Astronomy, Hunter College of the City University of New York,  
695 Park Avenue New York, New York 10065, USA*

<sup>4</sup>*Sandia National Laboratories, Albuquerque, New Mexico 87185, USA*

<sup>5</sup>*Department of Physics and Astronomy, University of California, Irvine, California 92697, USA*

(Dated: August 10, 2017)

Effects of induced optical polarization by Dirac electrons in graphene on the hybridization of radiative and evanescent fields is found. Such effects result in a localized polarization field which significantly modifies an incident surface-plasmon-polariton (SPP) field. This yields a high sensitivity to local dielectric environments and provides an investigative tool for molecules or proteins selectively bound with carbons. A scattering matrix is utilized with varied frequencies in the vicinity of the surface-plasmon (SP) resonance for the increase, decrease and even a full suppression of the polarization field, which enables accurate effective-medium theories to be constructed for Maxwell-equation finite-difference time-domain methods. Moreover, double peaks in the absorption spectra for hybrid SP and graphene-plasmon modes are significant only with a large conductor plasma frequency, but are overshadowed by a round SPP peak at a small plasma frequency as the graphene is placed close to conductor surface. These resonant absorptions facilitate the polariton-only excitations, leading to polariton condensation for a threshold-free laser.

PACS numbers: 73.20.Mf; 42.25.-p; 78.67.Wj; 78.68.+m

*Introduction:* It is known that when light is incident on a semiconductor, its energetic photons can elevate electrons from a valence band to a conduction band, leaving many electron-hole pairs in the system [1, 2]. Simultaneously, its electric-field component will further move aside these negatively (positively) charged electrons (holes) in opposite spatial directions. However, the remaining question is, *whether excited electrons or the holes exert an action back on the incident light?* The answer to this lies in the induced optical-polarization field as a collection of local dipole moments from many displaced electrons and holes [3, 4], which plays a role in scattering the electric-field component of the incident light [5, 6]. Therefore, the quantum nature of Dirac electrons [7–11] is expected to be retained in the effects of optical polarization on the incident light with a complex distribution of the Landau-damping regions in comparison with that for two-dimensional electron gases in a quantum well [12].

For a hybrid structure illustrated in Fig.1*a*, we encounter radiative field modes, such as photons and polaritons [13–17], as well as evanescent field modes, e.g., surface and graphene plasmons [18–20]. Research on optical responses of graphene electrons has been reported previously [20, 21], but most of those efforts have been limited to the radiation or grating-deflection field coupling. In contrast to a plane-wave-like external field, we explore the surface-plasmon-polariton near-field [22–24] coupling to graphene electrons with a different dispersion relation from the usual linear one, i.e.,  $\omega = qc$ , for free-space light. In our case, the graphene is brought very close to the surface of a conducting substrate so that the hybridization of radiative and evanescent fields can occur [25]. Consequently, the non-dispersive surface-plasmon mode is able to hybridize with radiative photon and polariton modes [13, 14], as well as with the spatially-localized graphene plasmon mode [12], as shown schematically in Fig.1*b*.

Such a distinctive dispersion relation of the hybrid quantum-plasmon modes should be experimentally observable in optical spectra [26–29]. The effective scattering matrix [30, 31] from such a coupled system is found to differ significantly from that for either the graphene or the conductor and it displays distinctive features from the retarded longitudinal Coulomb interaction [6] between electrons in the graphene and conductor. This scattering matrix can be employed for constructing an effective-medium theory [9, 32–35] and investigating the optical properties of inserted biomolecules and metamaterials between the graphene sheets and the surface of the conductor. Therefore, a locally environment-sensitive super-resolution near-field imaging can be developed for functionalized biomolecules bound to metallic nanodots and nanorods or even carbon atoms of graphene [36].

*Theory and Methods:* The structure under investigation is illustrated in Fig.1*a*, and consists of a thick conductor and a dielectric-embedded graphene above its surface. A surface-plasmon-polariton field (SPPF) can be excited by

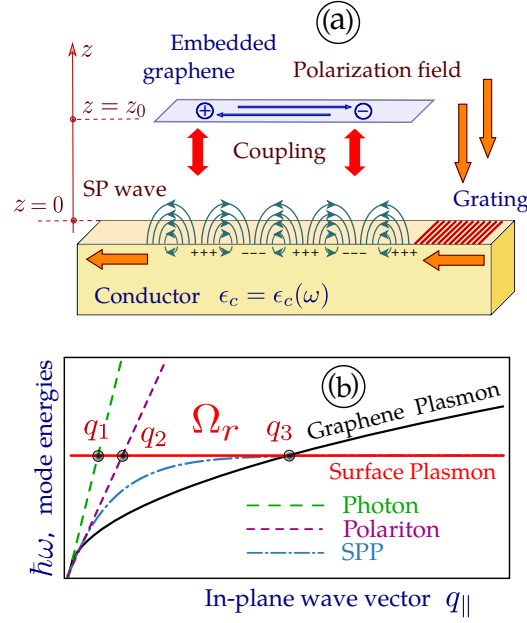


FIG. 1: (Color online) Schematic (a) for a thick conductor ( $z < 0$ ) with dielectric function  $\epsilon_c(\omega)$  and a graphene layer at  $z = z_0$  above its surface at  $z = 0$  which is embedded within a semi-infinite material, extending from  $z = 0$  to  $z = \infty$ , with dielectric constant  $\epsilon_d$ . The surface-plasmon-polariton field (SPPF) is excited by light incident on a grating. The propagating SPPF excites Dirac electrons in graphene and the induced graphene polarization modifies the SPPF by resonant scattering. Illustration (b) for energy dispersion of photons, polaritons, surface-plasmon polaritons (SPPs), graphene plasmons (G-Ps) and surface plasmons (SPs), where three labeled circles indicate the mode hybridizations.

incident light on a surface grating. This surface-propagating SPPF couples to Dirac electrons in graphene, and the induced polarization field from graphene acts back simultaneously on the SPPF as a resonant scatterer. The details about the derivations of Eqs. (1)-(4) below can be found from Ref. [37].

Using the Green's function approach, [5] we convert Maxwell's equation for the electric field  $\mathbf{E}(\mathbf{r}, \omega)$  into an integral equation in the spatial ( $\mathbf{r}$ ) domain, including a nonlocal source term to scatter the incident SPPF  $\mathcal{E}^{\text{inc}}(\mathbf{r}, \omega)$ , where  $\omega$  is the light frequency. After Fourier transforming this integral equation with respect to  $\mathbf{r}_{\parallel}$ , we obtain ( $\mu, \nu = 1, 2, 3$ )

$$E_{\mu}(\mathbf{q}_{\parallel}, \omega | x_3) = \mathcal{E}_{\mu}^{\text{inc}}(\mathbf{q}_{\parallel}, \omega | x_3) + \frac{\omega^2}{\epsilon_0 c^2} \sum_{\nu} g_{\mu\nu}(\mathbf{q}_{\parallel}, \omega | x_3, z_0) \mathcal{P}_{\nu}^s(\mathbf{q}_{\parallel}, \omega), \quad (1)$$

where  $\mathbf{r} = \{\mathbf{r}_{\parallel}, x_3\}$ ,  $x_3 = z_0$  denotes the graphene-sheet position, and  $g_{\mu\nu}(\mathbf{q}_{\parallel}, \omega | x_3, z_0)$  is the Fourier transformed Green's function matrix [6] which corresponds to a retarded coupling between graphene electrons to the incident SPPF. Using linear response theory [38], we obtain the graphene polarization field in Eq.(1)  $\mathcal{P}_{\nu}^s(\mathbf{q}_{\parallel}, \omega) = \epsilon_0 \chi_s^{(0)}(q_{\parallel}, \omega) (1 - \delta_{\nu 3}) E_{\nu}(\mathbf{q}_{\parallel}, \omega | z_0)$ , where  $\chi_s^{(0)}(q_{\parallel}, \omega) = e^2 \Pi_s^{(0)}(q_{\parallel}, \omega) / [\epsilon_0 (q_{\parallel}^2 - \epsilon_d \omega^2 / c^2)]$  [39], and  $\Pi_s^{(0)}(q_{\parallel}, \omega)$  is the density-density correlation function for graphene electrons [40-42]. The transverse and longitudinal electronic responses are associated with the magnetic and electric susceptibilities, respectively. The former is usually much weaker than the latter if no magnetic impurities are present in the graphene layer. In this paper, we will concentrate on the dominant scattering of the incident SPP electric field from the dielectric response of graphene while neglect the graphene diamagnetic response at the same time. The properties of the graphene diamagnetic response have been discussed before by using the lattice model. [43, 44] Setting  $x_3 = z_0$  in Eq.(1), we obtain a self-consistent equation for  $\mathbf{E}(\mathbf{q}_{\parallel}, \omega | z_0)$ . Furthermore, if  $\mathcal{E}^{\text{inc}}(\mathbf{q}_{\parallel}, \omega | z_0) = 0$  is assumed in this self-consistent equation, we obtain the dispersion equation for the hybrid plasmon modes, and the resulting dispersion relation  $\omega = \Omega(\mathbf{q}_{\parallel} | z_0)$ , as illustrated in Fig.1b, is determined from the real part of the secular equation  $\mathcal{D}et\{\vec{\mathcal{C}}(\mathbf{q}_{\parallel}, \omega | z_0)\} = 0$ , where  $\vec{\mathcal{C}}(\mathbf{q}_{\parallel}, \omega | z_0) = \delta_{\mu\nu} - (\omega/c)^2 g_{\mu\nu}(\mathbf{q}_{\parallel}, \omega | z_0, z_0) (1 - \delta_{\nu 3}) \chi_s^{(0)}(q_{\parallel}, \omega)$  is the complex coefficient matrix. After calculating the inverse of  $\vec{\mathcal{C}}$ ,  $\mathbf{E}(\mathbf{r}_{\parallel}, \omega | x_3)$  can be expressed explicitly as

$$E_{\mu}(\mathbf{r}_{\parallel}, \omega | x_3) = \mathcal{E}_{\mu}^{\text{inc}}(\mathbf{r}_{\parallel}, \omega | x_3) + \frac{\omega^2}{c^2} \int \frac{d^2 \mathbf{q}_{\parallel}}{(2\pi)^2} e^{i \mathbf{q}_{\parallel} \cdot \mathbf{r}_{\parallel}} \chi_s^{(0)}(q_{\parallel}, \omega) \\ \times \sum_{\nu} \left\{ g_{\mu\nu}(\mathbf{q}_{\parallel}, \omega | x_3, z_0) (1 - \delta_{\nu 3}) \left[ \sum_{\mu'} C_{\nu\mu'}^{-1}(\mathbf{q}_{\parallel}, \omega | z_0) \mathcal{E}_{\mu'}^{\text{inc}}(\mathbf{q}_{\parallel}, \omega | z_0) \right] \right\}. \quad (2)$$

From Eq.(2), the Fourier transformed scattering matrix [30] is readily determined to be given as

$$\alpha_{\mu\nu}^{\text{eff}}(\mathbf{q}_{\parallel}, \omega | x_3) = \frac{\omega^2}{c^2} \chi_s^{(0)}(q_{\parallel}, \omega) \sum_{\nu'} g_{\mu\nu'}(\mathbf{q}_{\parallel}, \omega | x_3, z_0) (1 - \delta_{\nu' 3}) C_{\nu'\nu}^{-1}(\mathbf{q}_{\parallel}, \omega | z_0). \quad (3)$$

Additionally, by using the calculated  $\mathbf{E}(\mathbf{r}_{\parallel}, \omega | z_0)$  in Eq.(2), the absorption coefficient  $\beta_{\text{abs}}(\omega | z_0)$  for the SPPF can be calculated [22, 45] based on the Lorentz function  $\alpha_L(\omega | z_0)$  given by

$$\alpha_L(\omega | z_0) = \frac{c}{\omega} \left| \sum_{\mu, \nu} \hat{e}_{\mu} C_{\mu\nu}^{-1}(\mathbf{k}_0, \omega | z_0) \left[ i \hat{k}_{\nu} \beta_3(\omega) - \hat{x}_{\nu} k_0(\omega) \right] e^{-\beta_3(\omega) z_0} \right| \\ \times \left( \frac{2\pi e^2}{\epsilon_0 \epsilon_r k_0} \right) \sqrt{1 - \frac{\epsilon_d \omega^2}{k_0^2 c^2} \left\{ \Pi_s^{(0)}(k_0, \omega) + [\Pi_s^{(0)}(k_0, -\omega)]^* \right\}}, \quad (4)$$

where  $\epsilon_r$  is the effective dielectric constant of the host material above the conductor surface in which the graphene layer is embedded and is approximately taken as the cladding-layer dielectric constant  $\epsilon_d$ ,  $\hat{\mathbf{e}}$  and  $\hat{\mathbf{k}}$  are the unit polarization and wave vectors of the SPPF,  $\hat{\mathbf{x}} = (0, 0, 1)$  is the spatial unit vector,  $\mathbf{k}_0 \equiv \text{Re}[k_0(\omega)] \hat{\mathbf{k}}$ ,  $\beta_3(\omega) = \sqrt{k_0^2(\omega) - \omega^2/c^2}$ ,  $k_0(\omega) = (\omega/c) \sqrt{\epsilon_d \epsilon_c(\omega) / [\epsilon_d + \epsilon_c(\omega)]}$ ,  $\epsilon_d$  is the cladding-layer dielectric constant,  $\epsilon_c(\omega) = \epsilon_s - \Omega_p^2 / [\omega(\omega + i0^+)]$  for the conductor, and  $\text{Re}[k_0(\omega)] \geq 0$  as well as  $\text{Re}[\beta_3(\omega)] \geq 0$  are assumed in treating the multi-value square roots. [37]

**Results and Discussions:** In our numerical calculations, we use the Fermi wave vector  $k_F = \sqrt{\pi n_0}$  as the scale for wave numbers,  $1/k_F$  for lengths, and  $E_F = \hbar v_F k_F$  for energies. The direction of SPPF propagation is chosen as  $\hat{\mathbf{k}} = (1, 0, 0)$  for simplicity, and we also set  $\epsilon_s = 13.3$ ,  $\epsilon_d = \epsilon_r = 2.4$ ,  $v_F = 1 \times 10^8$  cm/s, and  $n_0 = 5 \times 10^{11}$  cm<sup>-2</sup> for the doping density in graphene. Moreover, the half gap  $\Delta = 0$  is assumed unless it is stated in figure captions, and the resonant frequency  $\Omega_r = \Omega_p / \sqrt{\epsilon_s + \epsilon_d}$  will be given directly in figure captions.

For a retarded interaction between light and graphene electrons, both radiative and evanescent modes must be considered for the hybrid structure. The radiative modes include photons and polaritons, while the evanescent modes appear as surface-plasmon polaritons (SPPs), graphene plasmons (G-Ps), and surface plasmons (SPs). Figure 2 presents the real part of  $\mathcal{D}^{-1}(q_x, \omega | z_0) \equiv 1/\text{Det}[\vec{\mathcal{C}}(q_x, \omega | z_0)]$  for four chosen  $q_x$  ranges. It is clear from Fig.2a that in addition to the SPP mode, the hybridizations of both radiative photon and polariton modes with localized SPs (labeled as  $q_1$  and  $q_2$  in Fig.1b) appear in this very small  $q_x$  range. As the  $q_x$  range is slightly expanded in Fig.2b, the SPP mode in Fig.2a becomes fully developed, which is accompanied by a G-P mode at low energies. As the  $q_x$  range is further increased in Figs.2c and 2d, the G-P energy exceeds that of the SP. Consequently, the anticrossing of G-Ps with SPPs (labeled by  $q_3$  in Fig. 1b) is observed.

The  $z_0$  dependence in the secular equation highlights the nature of the distinctive evanescent coupling between SPPs and G-Ps. Here, the factor  $g_{\mu\nu}(q_x, \omega | z_0, z_0)$  plays the role of a retarded SPP coupling to a spatially-separated G-P, while  $\chi_s^{(0)}(q_x, \omega)$  corresponds to the G-P optical response. Therefore, their product represents the hybrid Dirac-SPP modes. By moving the graphene a bit further from the conductor surface, the anticrossing gap shrinks due to decreased retarded coupling. Simultaneously, the strengths of all the plasmon, polariton and photon modes increase by more than one order of magnitude due to loss suppression of these modes to the conductor.

The incident SPPF suffers not only Ohmic loss during its propagation along the conductor surface, but also absorption loss by its coupling to G-Ps. Figure 3 presents the absorption spectra  $\beta_{\text{abs}}(\omega | z_0)$  for various  $\Delta$  in (a) and chosen  $z_0$  in (b). From Fig.3a we find three absorption peaks for  $\Delta = 0$ , where two sharp ones correspond to G-Ps

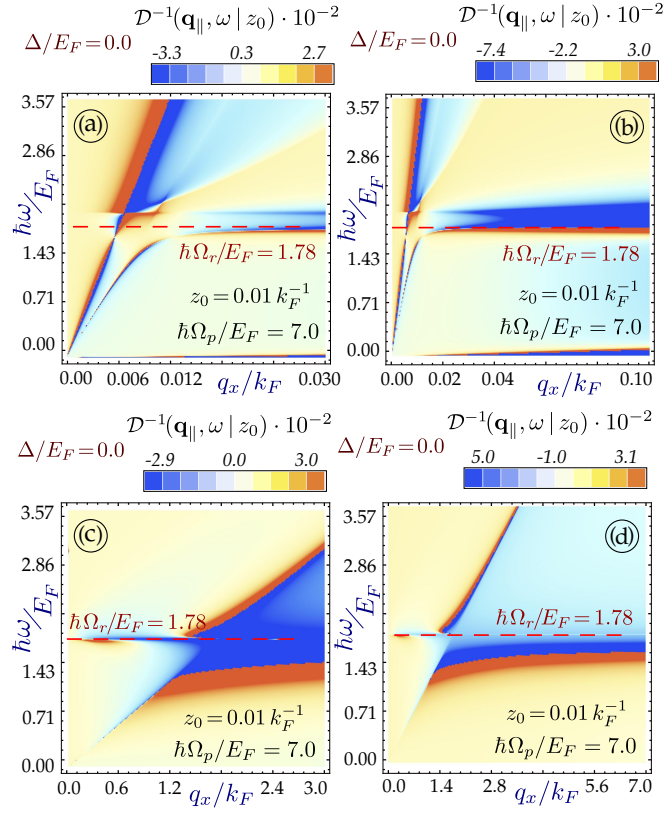


FIG. 2: (Color online) Density plots for the real part of  $\mathcal{D}^{-1}(q_x, \omega | z_0) \equiv 1/\text{Det}\{\hat{\mathcal{C}}(q_x, \omega | z_0)\}$  in four different  $q_x$  ranges growing from 0.03 to 7 with hybrid-plasmon dispersions indicated by jumps between positive (red) and negative (blue) peaks. Here,  $k_F z_0 = 0.01$ ,  $\hbar\Omega_r/E_F = 1.78$ .

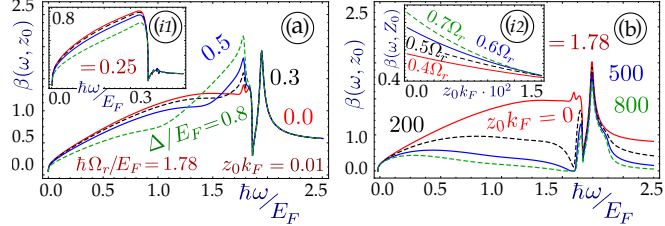


FIG. 3: (Color online) Absorption spectra  $\beta_{\text{abs}}(\omega | z_0)$  displayed in (a) with  $k_F z_0 = 0.01$  for  $\Delta/E_F = 0, 0.1, 0.3, 0.8$ , where  $\hbar\Omega_r/E_F = 1.78$  and  $0.25$  in its inset. In (b),  $\beta_{\text{abs}}(\omega | z_0)$  with  $\hbar\Omega_r/E_F = 1.78$ ,  $\Delta/E_F = 0$  for  $k_F z_0 = 0, 200, 500, 800$ , and its  $z_0$  dependence in the inset for  $\omega/\Omega_r = 0.4, 0.5, 0.6, 0.7$ .

(right) and SPs (left), as seen from Figs.2c and 2d, with a deep trough separating them for the opened anticrossing gap labeled as  $q_3$  in Fig. 1b. The lowest rounded peak is for SPP modes, as shown in Figs.2a and 2b, which is separated from the SP peak by a shallow dip labeled by  $q_2$  in Fig.1b. The absorption peak from the indistinguishable SPP and SP modes increases greatly in the inset of Fig.3a for a lower SP resonance  $\hbar\Omega_r/E_F = 0.25$  since the SPPF decay is largely eased at a much smaller  $q_x$ . The enhancement of the SPP absorption peak is also observed in Fig.3b for small  $z_0$  due to reduced SPPF decay. Moreover, we find from the inset of Fig. 3b that the decrease of  $\beta_{\text{abs}}(\omega | z_0)$  with increasing  $z_0$  becomes much more dramatic as  $\omega$  approaches  $\Omega_r$  with increased SPPF localization.

In addition to the SPPF optical absorption by G-Ps, resonant scattering of the SPPF from G-Ps also takes place, as described by Eq.(3). Figure 4 presents 3D plots for  $[\text{Re}\{\alpha_{11}^{\text{eff}}(q_x, \omega | x_3)\}]^{1/5}$  with four values for  $\omega$ , where the graphene is positioned relatively close to the surface. Here, the scattering matrix is  $\alpha_{\mu\nu}^{\text{eff}} \equiv \delta(E_\mu - \mathcal{E}_\mu^{\text{inc}})/\delta\mathcal{E}_\nu^{\text{inc}}$ , and its signs correspond to enhanced (+) or weakened (-) SPPF after light scattering with G-Ps. The left (right) and lower (upper) regions correspond to small (large)  $q_x$  and  $x_3$ , respectively. If both  $q_x$  and  $x_3$  are large, such scattering is significantly suppressed, leaving only a sizable and flat basin in the upper-right-hand corners of Figs.4a-4d. If  $q_x$  is very small, the

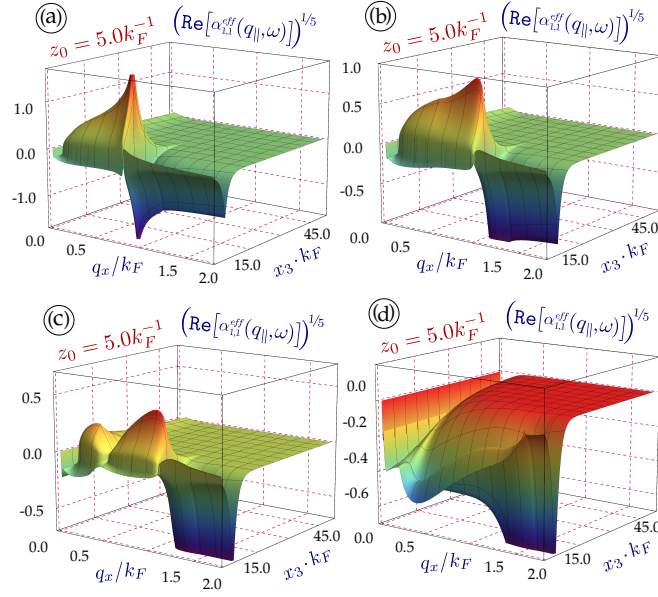


FIG. 4: (Color online) 3D plots for  $[\text{Re}\{\alpha_{11}^{\text{eff}}(q_x, \omega|x_3)\}]^{1/5}$  with  $\omega/\Omega_r = 0.7$  (a),  $0.8$  (b),  $0.9$  (c),  $1.0$  (d), where  $k_F z_0 = 5$ ,  $\hbar\Omega_r/E_F = 1.78$ .

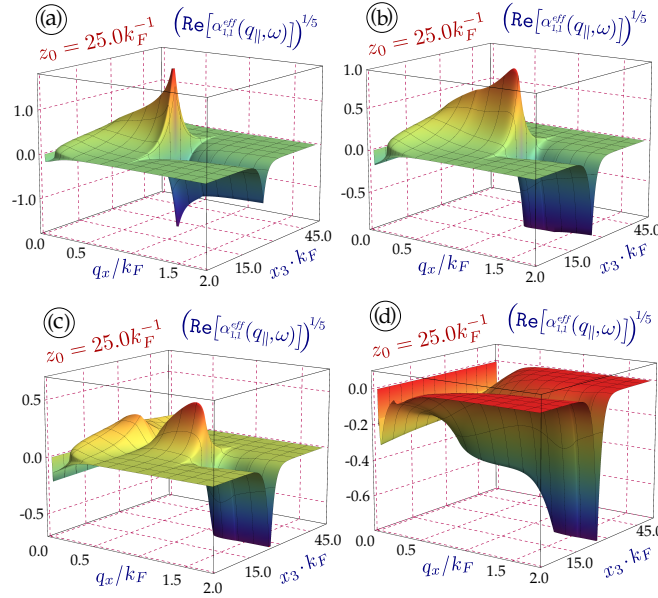


FIG. 5: (Color online) 3D plots for  $[\text{Re}\{\alpha_{11}^{\text{eff}}(q_x, \omega|x_3)\}]^{1/5}$  with  $\omega/\Omega_r = 0.7$  (a),  $0.8$  (b),  $0.9$  (c),  $1.0$  (d), where  $k_F z_0 = 25$ ,  $\hbar\Omega_r/E_F = 1.78$ .

photon and SPP radiative modes dominate, and then,  $\text{Re}\{\alpha_{11}^{\text{eff}}(q_x, \omega|x_3)\}$  remains negative and becomes independent of  $x_3$ . When  $q_x$  is intermediate, the SPP evanescent modes start entering in with increasing  $\omega$  up to  $\Omega_r$ . In this case, the positive peak strength is reduced and the peak coverage is squeezed into a smaller  $x_3$  region where the localization of SPPF is still insignificant. Even more, the positive peak is split into two islands at  $\omega = 0.9\Omega_r$  and it is eventually switched to a negative peak followed by a negative edge at  $\omega = \Omega_r$ . On the other hand, when  $q_x$  becomes very large for a strongly-localized SPPF, its scattering by G-P becomes negligible except for the region very close to the graphene as shown by the sharp negative edges in the lower-right-hand corners of Figs.4a-4d.

By moving the graphene further away from the conductor surface, as shown in Fig.5, we expect the scattering effects from G-Ps on the SPPF to be limited to a narrow area surrounding the graphene for large  $q_x$  values. Indeed,

when  $q_x$  is large, we find  $\text{Re}\{\alpha_{11}^{\text{eff}}(q_x, \omega|x_3)\} = 0$  for  $x_3$  far away from the graphene at  $z_0$  in the upper- and lower-right corners of Figs.5a-5d. For small  $q_x$  values, however, the positive peak appears, as in Fig.5, and its coverage crawls out along  $x_3 = z_0$  to a relative large  $q_x$  region followed by a negative sharp edge, although its peak strength decreases with increasing  $\omega$  towards  $\Omega_r$ . This extended region becomes separated from the positive peak at  $\omega = 0.9\Omega_r$  in Fig.5c to form an island, and both the positive peak and island disappear and are eventually replaced by negative sharp and stepped edges at  $\omega = \Omega_r$  in Fig.5d.

*Summary:* The effect of induced optical polarization on the hybridization of radiative and evanescent fields has been demonstrated by using a retarded interaction, which is seen as the hybrid dispersions for both radiative (small  $q_x$  range) and evanescent (large  $q_x$  range) field modes. Such an effect is rooted in the induced optical-polarization field from the Dirac plasmons, which resonantly redistributes an incident surface-plasmon-polariton field by scattering. The localization characteristics of such a retarded interaction ensure high sensitivity to dielectric environments surrounding graphene, including variations in the conducting substrate, cladding layer, electronic properties of embedded graphene, as well as the graphene distance from the conductor surface. This provides a unique advantage in wavelength-sensitive optical investigation of chemically-active molecules or proteins bound to carbon atoms in graphene [5, 6].

The optical probing tools discussed in this paper include either scattering or optical absorption of an incident electromagnetic field. For light scattering, we calculated the spatial-temporal dependence of a Fourier transformed scattering matrix, which clearly exhibits the scattering enhancement, weakening and even suppression as functions of both graphene separations ( $z_0$ ) from the conductor surface and wave numbers ( $q_x$ ) of the evanescent surface-plasmon-polariton field at several frequencies close to the localized surface-plasmon resonance. This derived scattering matrix lays the foundation for constructing an effective-medium theory commonly employed in finite-difference time-domain methods [46] for solving Maxwell's equations. For field absorption, the double peaks associated with hybrid surface and graphene plasmon modes on the high energy side are shown to be dominant for high conductor plasma frequencies and small graphene separations. However, the rounded peak on the low energy side plays the dominant role at low plasma frequencies. Additionally, this rounded peak shows that SPP modes can be greatly enhanced when graphene is moved close to the surface of the conductor. These unique features in resonant absorption enable the selective excitation of radiative polariton modes for their condensation and a threshold-free laser afterwards.

*Acknowledgments:* D.H. would like to thank the support from the Air Force Office of Scientific Research (AFOSR) under award number FA9550-14RV12COR.

- 
- [1] H. Haug and S. W. Koch, *Quantum Theory of the Optical and Electronic Properties of Semiconductors* (Fourth Edition, World Scientific Publishing Co. Pte. Ltd., 2004).
  - [2] F. Rossi and T. Kuhn, *Rev. Mod. Phys.* **74**, 895 (2002).
  - [3] M. Lindberg and S. W. Koch, *Phys. Rev. B* **38**, 3342 (1988).
  - [4] M. Kira and S. W. Koch, *Progress in Quantum Electronics* **30**, 155 (2006).
  - [5] D. H. Huang, M. M. Easter, G. Gumbs, A. A. Maradudin, S.-Y. Lin, D. A. Cardimona and X. Zhang, *Opt. Expr.* **22**, 27576 (2014).
  - [6] D. H. Huang, M. M. Easter, G. Gumbs, A. A. Maradudin, S.-Y. Lin, D. A. Cardimona, and X. Zhang, *Appl. Phys. Lett.* **104**, 251103 (2014).
  - [7] K. Novoselov, A. K. Geim, S. Morozov, D. Jiang, M. Katsnelson, I. Grigorieva, S. Dubonos, and A. Firsov, *Nature* **438**, 197 (2005).
  - [8] A. K. Geim and K. S. Novoselov, *Nature Materials* **6**, 183 (2007).
  - [9] K. K. Gomes, W. Mar, W. Ko, F. Guinea, and H. C. Manoharan, *Nature* **483**, 306 (2012).
  - [10] Y. Zhang, Y.-W. Tan, H. L. Störmer, and P. Kim, *Nature* **438**, 201 (2005).
  - [11] A. K. Geim, *Science* **324**, 1530 (2009).
  - [12] A. Iurov, G. Gumbs, D. H. Huang, and V. Silkin, *Phys. Rev. B* **93**, 035404 (2016).
  - [13] S. Christopoulos, G. B. H. von Högersthal, A. J. D. Grundy, P. G. Lagoudakis, A.V. Kavokin, J. J. Baumberg, G. Christmann, R. Butté, E. Feltn, J.-F. Carlin, and N. Grandjean, *Phys. Rev. Lett.* **98**, 126405 (2007).
  - [14] S. I. Tsintzos, N. T. Pelekanos, G. Konstantinidis, Z. Hatzopoulos, and P. G. Savvidis, *Nature* **453**, 372 (2008).
  - [15] P. Bhattacharya, B. Xiao, A. Das, S. Bhowmick, and J. Heo, *Phys. Rev. Lett.* **110**, 206403 (2013).
  - [16] C. Schneider, A. Rahimi-Iman, N. Y. Kim, J. Fischer, I. G. Savenko, M. Amthor, M. Lermer, A. Wolf, L. Worschech, V. D. Kulakovskii, I. A. Shelykh, M. Kamp, S. Reitzenstein, A. Forchel, Y. Yamamoto, and S. Höfling, *Nature* **497**, 348 (2013).
  - [17] E. L. Albuquerque and M. G. Cottam, *Phys. Rep.* **233**, 67 (1993).
  - [18] B. Wang, X. Zhang, F. J. García-Vidal, X. Yuan, and J. Teng, *Phys. Rev. Lett.* **109**, 073901 (2012).
  - [19] M. Liu, X. Yin, and X. Zhang, *Nano Letters* **12**, 1482 (2012).
  - [20] M. Liu, X. Yin, E. Ulin-Avila, B. Geng, T. Zentgraf, L. Ju, F. Wang, and X. Zhang, *Nature* **474**, 64 (2011).

- [21] F. Koppens, T. Mueller, P. Avouris, A. Ferrari, M. Vitiello, and M. Polini, *Nature Nanotechnology* **9**, 780 (2014).
- [22] A. A. Maradudin and D. L. Mills, *Phys. Rev. B* **11**, 1392 (1975).
- [23] M. G. Cottam and A. A. Maradudin, “Surface linear response functions”, in *Surface Excitations*, eds. V. M. Agranovich and R. Loudon (North-Holland, Amsterdam, 1984), pp. 1-194.
- [24] J. M. Pitarke, V. M. Silkin, E. V. Chulkov, and P. M. Echenique, *Rep. Prog. Phys.* **70**, 1 (2007).
- [25] A. V. Zayats, I. I. Smolyaninov, and A. A. Maradudin, *Phys. Rep.* **408**, 131 (2005).
- [26] M. S. Tame, K. R. McEnery, S. K. Özdemir, J. Lee, S. A. Maier, and M. S. Kim, *Nature Physics* **9**, 329 (2013).
- [27] F. de León-Pérez, G. Brucoli, F. J. Garca-Vidal, and L. Martín-Moreno, *New J. Phys.* **10**, 105017 (2008).
- [28] A. N. Grigorenko, M. Polini, and K. S. Novoselov, *Nature Photonics* **6**, 749 (2012).
- [29] D. N. Basov, M. M. Fogler, A. Lanzara, F. Wang Y. Zhang, *Rev. Mod. Phys.* **86**, 959 (2014).
- [30] D. S. Saxon, *Phys. Rev.* **100**, 1771 (1955).
- [31] F. J. García de Abajo, *Rev. Mod. Phys.* **79**, 1267 (2007).
- [32] J. van Kranendonk and J. E. Sipe, “Foundations of the macroscopic electromagnetic theory of dielectric media”, in *Progress in Optics XV*, ed. E. Wolf (New York: North-Holland, 1977), Chap. 5.
- [33] G. D. Mahan and G. Obermair, *Phys. Rev.* **183**, 834 (1969).
- [34] J. Sipe and J. van Kranendonk, *Phys. Rev. A* **9**, 1806 (1974).
- [35] W. Lamb, D. M. Wood, N. W. Ashcroft, *Phys. Rev. B* **21**, 2248 (1980).
- [36] M. Wojcik, M. Hauser, W. Li, S. Moon, and K. Xu, *Nature Communications* **6**, 7384 (2015).
- [37] D. H. Huang, O. Roslyak, G. Gumbs, W. Pan and A. A. Maradudin, *Proc. SPIE* **9961**, 996104 (2016).
- [38] G. Gumbs and D. H. Huang, *Properties of Interacting Low-Dimensional Systems* (John Wiley & Sons, 2011), Chap. 2.
- [39] D. H. Huang, G. Gumbs and O. Roslyak, *Applied Optics* **52**, 755 (2013).
- [40] B. Wunsch, T. Stauber, F. Sols, and F. Guinea, *New J. Phys.* **8**, 318 (2006).
- [41] P. Pyatkovskiy, *J. Phys.: Condensed Matter* **21**, 025506 (2008).
- [42] O. Roslyak, G. Gumbs and D. H. Huang, *J. Appl. Phys.* **109**, 113721 (2011).
- [43] A. Principi, M. Polini, and G. Vignale, *Phys. Rev. B* **80**, 075418 (2009).
- [44] T. Stauber and G. Gómez-Santos, *Phys. Rev. B* **82**, 155412 (2010).
- [45] D. H. Huang and Y. Zhao, *Phys. Rev. A* **51**, 1617 (1995).
- [46] A. F. Oskooi, D. Roundy, M. Ibanescu, P. Bermel, J. D. Joannopoulos, S. G. Johnson, *Computer Physics Communications* **181**, 687 (2010).